

Development of a High-Voltage Output DAC System for Fast Ion-Shuttling

T. Oshio,¹ R. Nishimoto,^{1,2} T. Higuchi,³ K. Hayasaka,^{2,1} K. Koike,⁴ S. Morisaka,^{5,6} T. Miyoshi,^{6,5,4} R. Ohira,⁶ and U. Tanaka^{1,5,2}

¹*Graduate School of Engineering Science, Osaka University, 1-3 Machikaneyama, Toyonaka, Osaka, Japan.*

²*National Institute of Information and Communications Technology, 588-2, Iwaoka, Nishi-ku, Kobe, Hyogo, Japan.*

³*Institute for Integrated Radiation and Nuclear Science, Kyoto University, 2, Asashiro-Nishi, Kumatori-cho, Sennan-gun, Osaka, Japan.*

⁴*e-trees. Japan, Inc., Daiwaunyu Building 2F, 2-9-2 Owadamachi, Hachioji, Tokyo, Japan.*

⁵*Center for Quantum Information and Quantum Biology, Osaka University, 1-2 Machikaneyama, Toyonaka, Osaka, Japan.*

⁶*QuEL, Inc., Daiwaunyu Building 3F, 2-9-2 Owadamachi, Hachioji, Tokyo, Japan.*

(*Electronic mail: utako@ee.es.osaka-u.ac.jp)

(Dated: 11 December 2024)

The quantum charge-coupled device (QCCD) is one of the notable architectures to achieve large-scale trapped-ion quantum computers. To realize QCCD architecture, ions must be transported quickly while minimizing motional excitation. High-voltage sources are necessary to achieve such high-quality ion transport through a high secular frequency. In this study, we report the development of an FPGA-based DAC system with an output voltage range of ± 50 V and demonstrate its effectiveness in ion transport operations. By optimizing the voltage sets for ion transport, we experimentally confirm that the developed DAC system, when operated with an output range of ± 50 V, achieves more than twice the secular frequency attainable when its output range is restricted to ± 10 V, a limit commonly associated with conventional DACs. The developed DAC system has good potential to enable fast ion transport with minimal motional excitation, thereby reducing processing times in QCCD-based quantum computers.

I. INTRODUCTION

Trapped-ion qubits¹ are one of the most promising physical platforms for realizing quantum computers due to their long coherence times² and high-fidelity quantum gate operations³⁻⁵. So far, quantum computers with tens of trapped-ion qubits have been developed^{6,7}. However, scaling to larger systems remains a significant challenge.

One promising approach for realizing large-scale trapped-ion quantum computers is the quantum charge-coupled device (QCCD) architecture⁸. In this architecture, time-dependent voltages are applied to the trap electrodes to shuttle trapped-ion qubits between multiple operational regions, such as those for quantum gates, memory, state preparation, and measurement. Since the initial proposal by Kielpinski *et al.*⁸, numerous advancements have been made, and the QCCD architecture continues to be actively studied in the community⁹⁻¹².

A key technical challenge in realizing a QCCD-based quantum computer is achieving fast ion transport. The processing time of a QCCD trapped-ion quantum computer is largely dominated by ion cooling, the longest operation in the sequence. This is followed by shuttling operations, which highlights the importance of increasing the speed of the shuttling ions without heating of the motional state of the ions¹⁰.

Typically, the speed of the shuttling ions is constrained by the secular frequency^{13,14}, when the ion is transported adiabatically. Therefore it is key to increase the secular frequency to enable faster ion transport. In addition to adiabatic transport, diabatic transport techniques have also been extensively studied¹⁵⁻¹⁷. Simulations have shown that higher voltages al-

low faster diabatic transport with minimal motional excitation¹⁸. Thus, it is essential to increase the secular frequency for adiabatic transport operations, and a high-voltage output DAC system is essential for diabatic transport operations. To date, a digital-to-analog converter (DAC) system with an output range of ± 40 V has been developed and demonstrated for shuttling operations⁹.

In this study, we report the development of a field programmable gate array (FPGA)-based DAC system, which is capable of generating an output range of ± 50 V. We integrated this DAC system into our trapped-ion setup and conducted experimental assessments to evaluate its performance. Using the DAC system, we trapped a $^{40}\text{Ca}^+$ ion with voltage sets optimized with quadratic programming in a planar trap and measured a secular frequency exceeding $2\pi \times 500$ kHz. In contrast, when the DAC system's output range was limited to ± 10 V, which is a typical output limitation of conventional DACs, the achievable secular frequency was restricted to $2\pi \times 240$ kHz. The experimental demonstration was performed with our specific ion trap structure, but numerical simulations showed that the accessible secular frequency range was extended for other ion trap structures with different dimension and operating parameters. This advancement represents a step towards faster and more precise ion transport in large-scale QCCD quantum computers.

This paper is organized as follows. Section II describes the experimental equipment and protocol for ion-shuttling operations. Section III provides detailed information on the developed DAC system and its performance. In Section IV, we experimentally assess the performance of the developed DAC

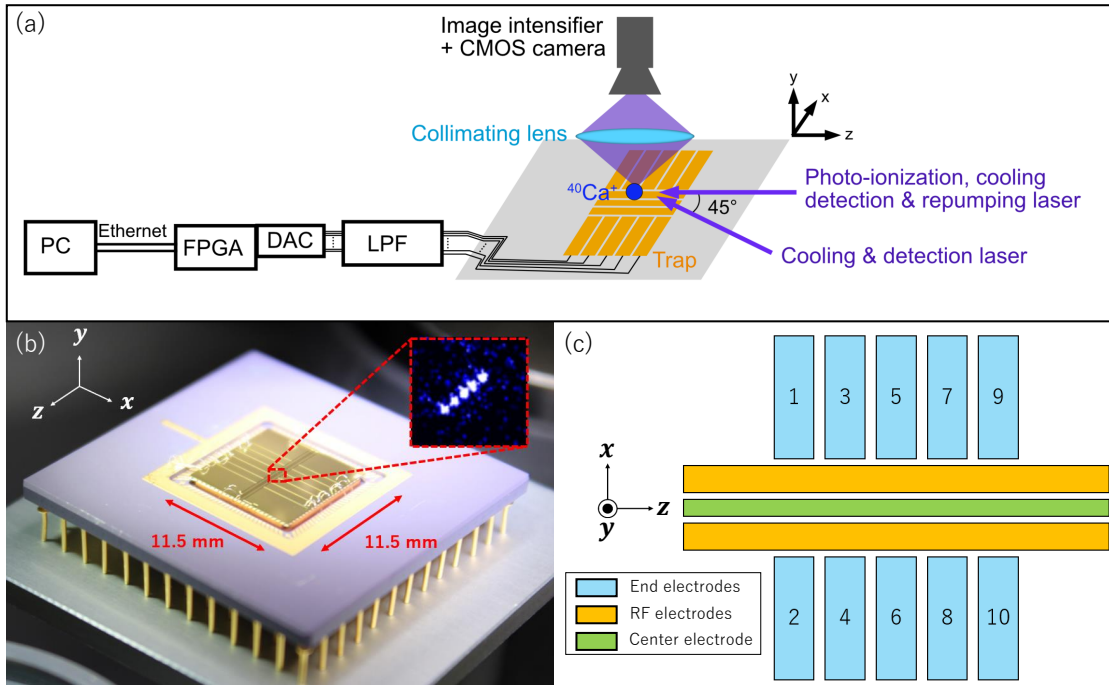


FIG. 1. Overview of the experimental setup. (a) Block diagram of the experimental setup. (LPF: Low-Pass Filter) (b) Planar ion trap used in this study with a fluorescence image of five $^{40}\text{Ca}^+$ ions. The size of the trap chip is 11.5 mm square and placed in vacuum system. (c) Schematic of the trap structure (not to scale). Details of the electrode dimensions are described in the main text.

system. Finally, Section V presents the conclusions of this study.

II. EXPERIMENTAL METHOD

In this section, we first provide an overview of the experimental setup, focusing on the trap electrode and laser configuration. Next, we explain the method of optimizing the voltage sets for the ion-shuttling operations and that of measuring the secular frequency of the trapped ions.

A. Planar ion trap

The overview of the experimental setup is shown in Fig. 1(a). All experiments presented in the study were performed using the planar ion trap shown in Fig. 1(b). This trap is housed in an ultra-high vacuum system with a vacuum level of approximately 6.7×10^{-8} Pa (5×10^{-10} Torr). The planar trap consists of two RF electrodes and eleven DC electrodes, including ten end electrodes and a center electrode, as shown in Fig. 1(c). The dimensions of each electrode are as follows: the end electrodes are $5075 \mu\text{m} \times 1000 \mu\text{m}$, the RF electrodes are $300 \mu\text{m} \times 11000 \mu\text{m}$, and the center electrode is $100 \mu\text{m} \times 11000 \mu\text{m}$. The gap between the RF and DC electrodes is $50 \mu\text{m}$, and the gap between adjacent DC electrodes is $25 \mu\text{m}$. The RF and end electrodes provide confinement along the x -direction, while the RF, center and parts

of the end electrodes contribute to confinement along the y -direction. The end electrodes provide confinement along the z -direction. The ions are trapped above the center electrode.

We applied RF voltage at $2\pi \times 24.31$ MHz to the RF electrodes, generated by an oscillator and amplified to approximately $200 V_{\text{pp}}$ using an amplifier and a helical resonator. As shown in Fig. 1(a), all of the DC voltages were controlled by the DAC system (see section III for details of the system). The signals from the DAC system passed through a low-pass filter (LPF) to suppress noise and smooth rapid voltage changes. The typical trapping voltages for the end electrodes were $[V_1, V_2, \dots, V_{10}] = [0, 0, 10, 10, 0, 0, 10, 10, 0, 0]$ V. Here, V_1, V_2, \dots, V_{10} refer to the voltages applied to the end electrodes labeled in Fig. 1(c). The typical trapping voltage for the center electrode was 3 V. Using these trapping conditions and an analytical solution¹⁹ of the trap potential, which was produced by rectangular electrode, we estimated the secular frequencies to be approximately $(\omega_x, \omega_y, \omega_z) \approx 2\pi \times (2.0, 2.9, 0.34)$ MHz, where ω_i denotes the secular frequency along the i -axis, and the trapping height from the trap surface was approximately $190 \mu\text{m}$.

B. Laser beam configuration and fluorescence detection of ions

In Fig. 1(a), the laser beam configuration and detection system are depicted. In this study, all experiments were performed using $^{40}\text{Ca}^+$ ions. $^{40}\text{Ca}^+$ ions are isotope-selectively

produced using a photoionization method^{20,21}. Laser beams at 423 nm and 375 nm were applied to a neutral Ca atomic beam. The ions were Doppler-cooled by applying optical beams at 397 nm and 866 nm. The 397 nm, 423 nm, and 866 nm lasers were homemade external-cavity diode lasers, while a commercially available laser source was used for the 375 nm laser (Nichia NDU4116). The wavelengths of these laser beams were measured using a wavemeter (HighFinesse WS7), calibrated with a He-Ne laser (Thorlabs HRS015B). The ions were detected by irradiating a 397 nm laser beam onto the $^{40}\text{Ca}^+$ ions, exciting the $^2S_{1/2} \leftrightarrow ^2P_{1/2}$ transition. The fluorescence from trapped ions collimated by the lens and amplified with an image intensifier (Hamamatsu Photonics C9016-02) was detected by a CMOS camera (Thorlabs DCC3240M).

C. The Voltage optimization for ion-shuttling operations

For the ion-shuttling operation, we attempted to find the voltage sets that produce the electrostatic potential Φ while minimizing the difference between Φ and target potential Φ_{target} :

$$\text{Minimize : } \|\Phi - \Phi_{\text{target}}\|^2. \quad (1)$$

To solve such a minimization problem and determine the voltage sets, we used quadratic programming.²² Quadratic programming is a type of nonlinear optimization method that minimizes an objective function:

$$\text{Minimize : } \frac{1}{2}x^T Px + q^T x, \quad (2)$$

where matrix P and vector q are determined by the desired potential (details will be discussed later). x is a vector, representing the set of voltages, which is defined as

$$x^T = (V_a, V_b, V_c, V_d, V_e). \quad (3)$$

In our optimization, we imposed a constraint that each pair of electrodes with the same z -component was set to be the same voltage, such that $V_1 = V_2 = V_a$, $V_3 = V_4 = V_b$, $V_5 = V_6 = V_c$, $V_7 = V_8 = V_d$, $V_9 = V_{10} = V_e$. We optimized the voltages for ion transport from the start point to the end point by adjusting the voltages N times. The start position is represented as step 0, and the end point as step N . At each step k ($0 \leq k \leq N$), we express the ion position as z_k , which is corresponding to the null point of the electrostatic potential. The electrostatic potential Φ_k around $z = z_k$ can be approximated by a harmonic potential along the z -axis:

$$\Phi_k(z) = \frac{m\omega_z^2}{2e}(z - z_k)^2, \quad (4)$$

where m is the ion mass and e is the elementary charge. In this experiment, z_k is defined as:

$$z_k = z_0 + (z_N - z_0)\sin^2\left(\frac{\pi k}{2N}\right), \quad (5)$$

to smoothen the transport speed changes and thereby, reduce the heating of the motional states of the ion.

To generate the required potential along the z -axis, we define the basis function $\phi_{\text{base}_i}(z)$ as the potential generated when a unit voltage is applied to each electrode pair $i \in (a, b, c, d, e)$. The potential at each step is a linear combination of these basis functions, with the optimization range (L) for each step k set as $z_{\text{min}} = z_k - L/2$ and $z_{\text{max}} = z_k + L/2$. The matrices v and f are defined as:

$$v = \begin{pmatrix} \phi_{\text{base}_a}(z_{\text{min}}) & \cdots & \phi_{\text{base}_a}(z_{\text{max}}) \\ \vdots & & \vdots \\ \phi_{\text{base}_e}(z_{\text{min}}) & \cdots & \phi_{\text{base}_e}(z_{\text{max}}) \end{pmatrix}, \quad (6)$$

$$f = (\Phi_k(z_{\text{min}}), \dots, \Phi_k(z_{\text{max}})). \quad (7)$$

Using v and f , P and q can be expressed as:

$$P = 2v \cdot v^T, \quad (8)$$

$$q = -2v \cdot f^T. \quad (9)$$

Additionally, the full scale range (FSR) of the DAC imposes restrictions on x , which are incorporated into the optimization by defining G and h as:

$$G = \begin{pmatrix} 1 & 0 & 0 & 0 & 0 \\ -1 & 0 & 0 & 0 & 0 \\ 0 & 1 & 0 & 0 & 0 \\ 0 & -1 & 0 & 0 & 0 \\ 0 & 0 & 1 & 0 & 0 \\ 0 & 0 & -1 & 0 & 0 \\ 0 & 0 & 0 & 1 & 0 \\ 0 & 0 & 0 & -1 & 0 \\ 0 & 0 & 0 & 0 & 1 \\ 0 & 0 & 0 & 0 & -1 \end{pmatrix}, h = \frac{(\text{FSR})}{2} \begin{pmatrix} 1 \\ 1 \\ 1 \\ 1 \\ 1 \\ 1 \\ 1 \\ 1 \\ 1 \\ 1 \end{pmatrix}. \quad (10)$$

We included these inequality constraints as:

$$Gx \leq h. \quad (11)$$

With these parameters, the voltage set x was optimized using common Python packages. Fig. 2(a) and Fig. 2(b) show the optimized result with an FSR of 20 V (DAC output range of ± 10 V) and 100 V (DAC output range of ± 50 V), respectively. In both cases, the target secular frequency ω_z was set as $2\pi \times 500$ kHz, with a transport distance of 200 μm . In Fig. 2(a), the blue, red and purple lines overlapping at approximately +10 V are due to the voltage restriction. Using the optimized voltage sets, we successfully performed ion shuttling 10,000 times, with each step duration set to 100 μs in the experimental setup described above.

D. Measurement of secular frequency

Here, we describe the method of measuring the secular frequency of a single trapped ion at each step during the ion-shuttling operation. The secular frequency was measured by

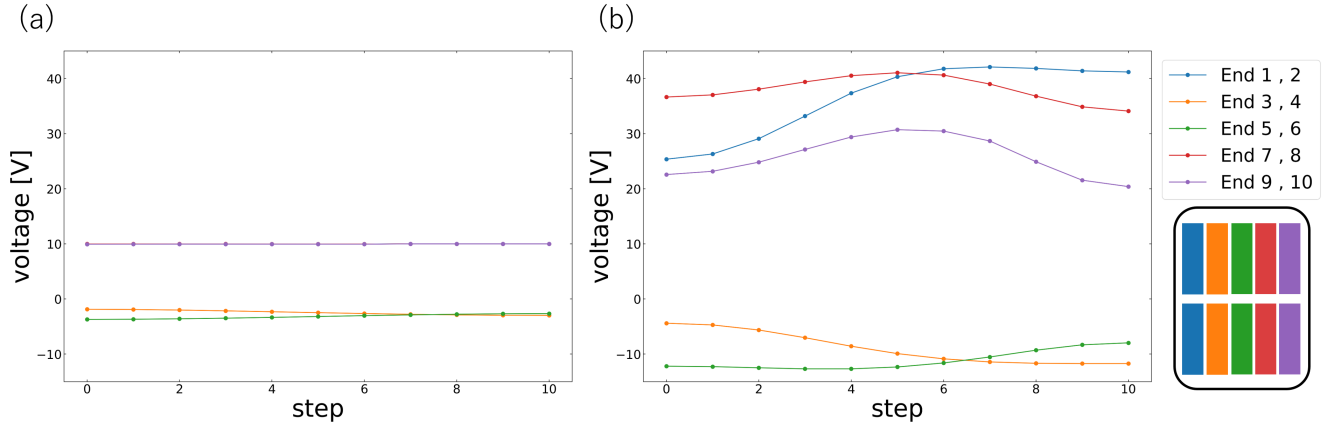


FIG. 2. Optimized voltage sets with (a) an FSR of 20 V (DAC output range of ± 10 V) and (b) an FSR of 100 V (DAC output range of ± 50 V). The schematic in the lower right shows the arrangement of the end electrodes, corresponding to Fig. 1(c), with colors matching the plot curves and marks. The voltage sets were calculated using quadratic programming for a constant secular frequency $\omega_z = 2\pi \times 500$ kHz.

observing the resonance of the ion motion by sweeping the frequency of an RF excitation and observing an increase in the ion width on resonance. We applied an oscillating voltage to one electrode of the trap (End 6) to resonantly excite the motion of a single ion. When the resonance happened, the width of the ionic motion was enlarged in the image detected by the CMOS camera. Large amplitude of an oscillating voltage led the trapped ions to escape. Thus, we set the amplitude to 30 mV_{pp} . We swept the frequency of an oscillating voltage over a range of approximately 15 kHz with a step of 0.1 kHz and recorded the ion image to extract the ion width at the same time. We then fitted the results with a Lorentzian to obtain the secular frequency.

The secular frequency can be measured by observing a decrease in the ion fluorescence with a photo-multiplier tube. However, the increase in the ion width is observable before decreasing the amount ion fluorescence is observed²³. Furthermore, a single CMOS camera is sufficient even observe multiple trapped ions.

The result of measuring the secular frequency is shown in Fig. 3. The secular frequency was calculated by fitting the ion fluorescence data (blue dots) with a Lorentzian (yellow curve). The peak of the fitted curve (red dashed line) was identified as the secular frequency, ω_z . To obtain these results, the experimental sequence was repeated ten times, and the full width at half maximum (FWHM) was determined as the average of the fluorescence profiles. The ion fluorescence was acquired with the camera exposure time set to 10 ms. From this measurement, the secular frequency ω_z was determined to be $2\pi \times 276.6$ kHz.

III. DEVELOPMENT OF A HIGH-VOLTAGE DAC SYSTEM

The overview of the developed DAC system is shown in Fig. 4. The system includes an FPGA System on Chip (SoC) (Digilent, Zedboard) and multiple DACs (ADI, AD3542R) connected via Dual SPI. Multiple BlockRAMs store output

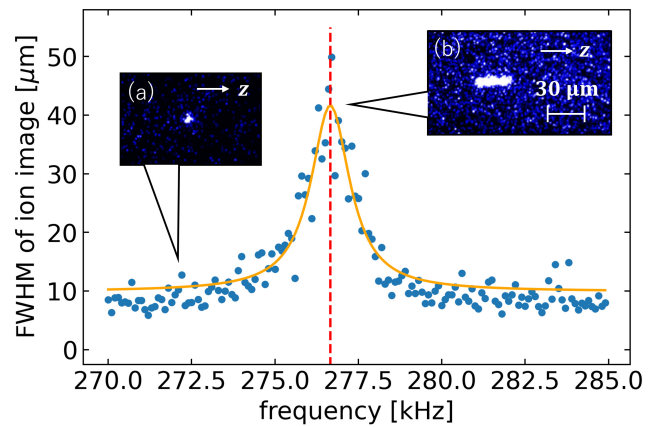


FIG. 3. Full Width at Half Maximum (FWHM) of ion fluorescence as a function of the frequency of the signal applied to the end electrode (End 6). The signal frequency was swept in increments of 0.1 kHz. The FWHM data (blue dots) were fitted with a Lorentzian (yellow curve), with the peak position (red dashed line) indicating the secular frequency ω_z , determined to be $2\pi \times 276.6$ kHz. The data corresponds to shuttling step 0 when the voltage output range is limited to ± 10 V. The insets show fluorescence images of the ion (a) off-resonance and (b) on-resonance.

pattern data for the corresponding DACs. To control the DAC output voltage, the user stores the pattern into the BlockRAMs using a Python script running on an ARM processing system within the Zynq. The design specification of the developed DAC system is shown in Table.I.

Fig. 5 shows the internal architecture of the sequencer. This sequencer generates waveforms by reading data from the Wave Pattern Storage based on entries in the Chunk Storage. The module starts running when the kick signal is asserted, during which the busy signal remains active. The module generates waves according to the specified parameters, but the users can stop the module at any time by assert-

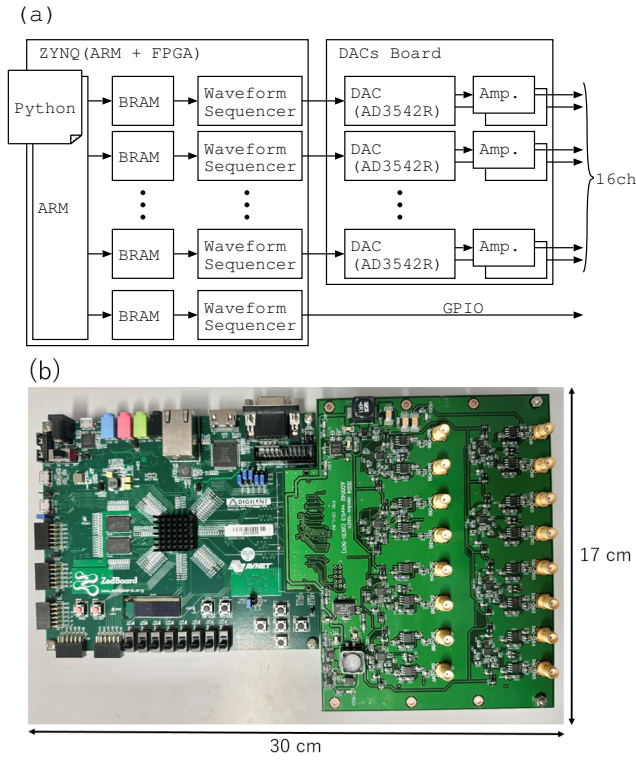


FIG. 4. Overview of the developed DAC system. The system consists of an FPGA board (Zedboard) and a custom-designed analog signal output board. (a) Block diagram of the developed DAC system. (b) Photograph of an FPGA board and an analog output board.

TABLE I. Design specifications of the output signal.

Number of channels	16
Voltage range	+/- 50V
Output voltage resolution	16-bit or 12-bit
Maximum update rate	16 MUPS
Maximum threwh rate	20 V/ μ s

ing the `force_stop` signal. Only when the module asserts `wave_valid`, the `wave_out` signal is valid.

The definition of the wave patterns is shown in Fig. 6. The waveform is generated by combining multiple chunks defined by the parameters of the Chunk Storage. Each Chunk Storage entry contains `chunk_length`, `chunk_offset`, and `chunk_repetition`. The parameters `chunk_offset` and `chunk_length` specify the start address and length of the Wave Pattern Storage to read for each chunk. The parameter `chunk_repetition` specifies the number of repetitions of the chunk. The number of entries read from the Chunk Storage is given by `ctrl_length`, and `repetition` specifies the number of repetitions for reading the sequence of the chunks.

The multiple DACs convert the generated waveform into analog signals, which are then amplified to a range of ± 50 V using high-throughput operational amplifiers (OP-amps). Fig. 7 illustrates the schematic of a DAC and two amplifiers. The DAC used in this system, the AD3542R, features two output ports, each connected to an independent OP-amps

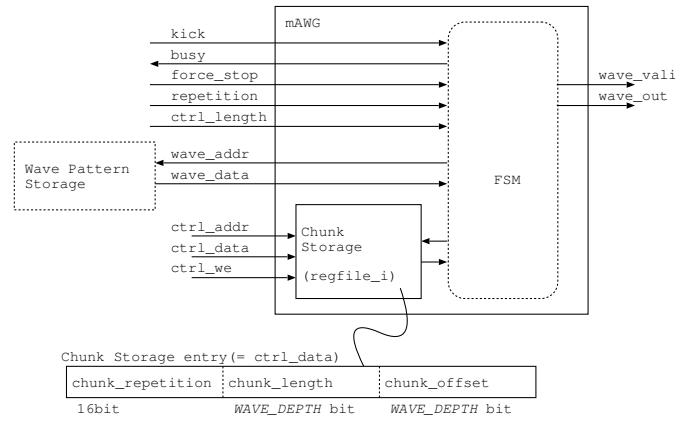


FIG. 5. Overview of the waveform sequencer. This sequencer generates waveforms by reading data from Wave Pattern Storage according to rules defined in Chunk Storage. The generated waveform is illustrated in Fig. 6.

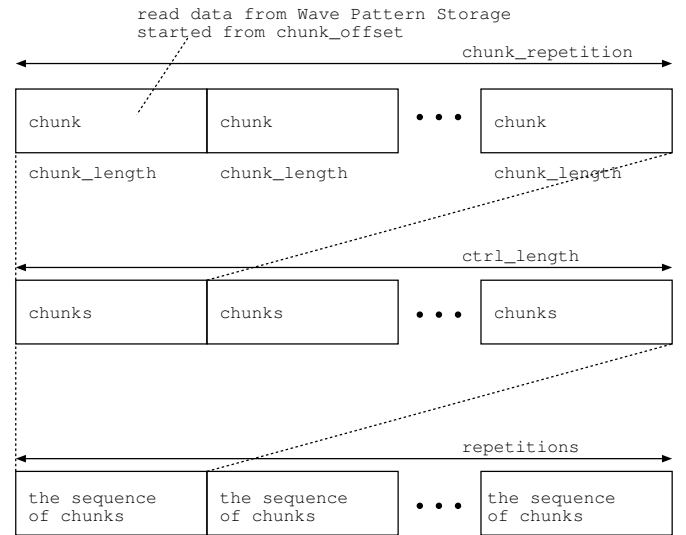


FIG. 6. Overview of the waveform pattern. The memory footprint of the defined waveform is reduced by utilizing repetition patterns within the waveform.

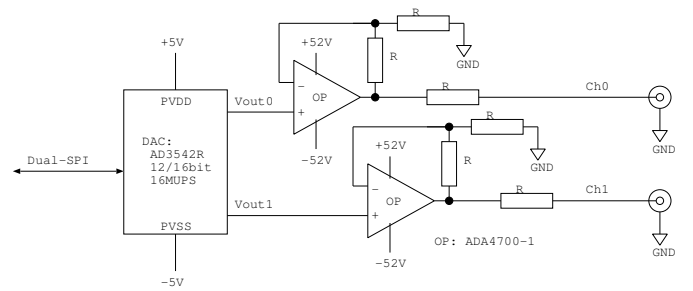


FIG. 7. Schematic of the analog output module used in this study. The Op-amps (ADA4700) contributes to the realization of the DAC output range of ± 50 V.

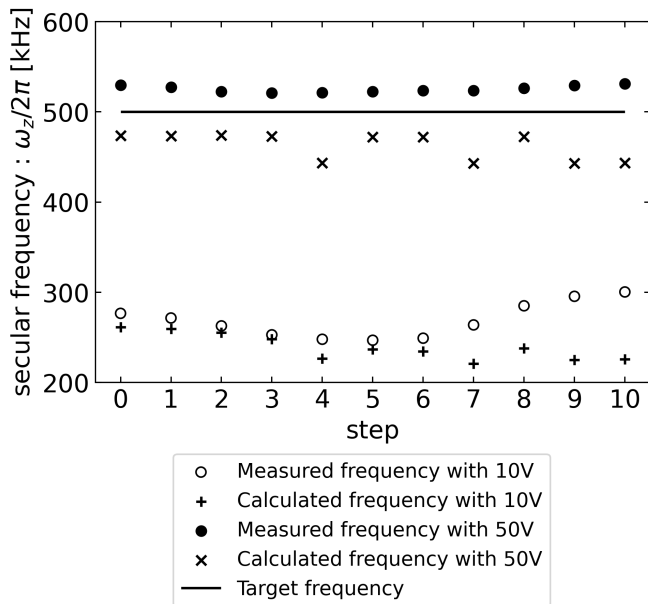


FIG. 8. Measured secular frequencies of ions trapped at each step of the shuttling operation using the voltage sets shown in Fig. 2. The results are presented for the DAC’s output range limited to ± 10 V (white dots) and ± 50 V (black dots). The size of the error bars is within the marker size. Calculated secular frequencies based on the used voltage sets are also shown for the DAC’s output range limited to ± 10 V (plus markers) and ± 50 V (cross markers). The horizontal line indicates the target ω_z used for optimization.

(ADA4700). While the DAC provides a high slew rate, the overall slew rate of the analog signal output is limited by the OP-amp’s slew rate.

IV. RESULT AND DISCUSSION

Using the voltage sets derived in subsection II C, we trapped $^{40}\text{Ca}^+$ ions at each step i.e., at each position during ion transport, and measured ω_z by the ion resonance experiments described in subsection II D.

The measurement results are shown in Fig. 8. The horizontal line at $\omega_z = 2\pi \times 500$ kHz indicates the optimization target. It is experimentally observed that the secular frequency cannot achieve the target secular frequency when the DAC output range is limited to ± 10 V. This limitation arises because many of the optimized voltage values shown in Fig. 2(a) reach the ± 10 V limit. In contrast, with a ± 50 V DAC output, the measured secular frequencies closely match the target frequency. The discrepancies between the measured results and the target or calculated values are likely due to external factors such as floating electric fields from Ca atom deposition on the trap surface.

The disagreement between the target secular frequency and achieved secular frequency may be attributed to the difference between the objective function values in the optimization process and the potentials calculated from the optimized voltage

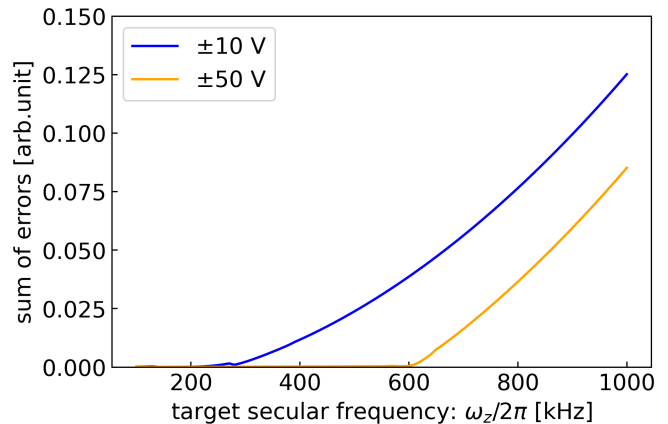


FIG. 9. Estimation of the optimization error when the output voltage restriction of ± 10 V (blue curve) and ± 50 V (orange curve). The error is calculated as the difference between the target potential and the potential generated by the optimized voltage sets.

sets. This difference arises due to the constraints imposed by the output voltage range. To evaluate this, we calculated the sum of errors within the optimization range for the target secular frequencies varying from 100 kHz to 1 MHz in increments of 10 kHz. The results are shown in Fig. 9. The range where the sum of the errors remains nearly zero is broader for the ± 50 V restriction compared to the ± 10 V restriction. Furthermore, at the target frequency of $2\pi \times 500$ kHz, the sum of errors is significantly smaller for the ± 50 V restriction than for the ± 10 V restriction. These calculated results correlate well with the experimental results shown in Fig. 8.

Motional heating of the ions during the shuttling operations is another important issue of the QCCD architecture. The scope of the present study is to confirm the increase in the secular frequency by extending the DAC output range in an actual setup, and experimental evaluation of the noise characteristics will be performed as the next step. The experimental observation of the absence of ion loss during the shuttling process as many as 10,000 times indicates that notable heating is not evoked by our high voltage DAC.

V. CONCLUSION

In this study, we developed an FPGA-based DAC system with an analog output voltage range of ± 50 V and successfully demonstrated its application to ion transport operations. We used quadratic programming to optimize voltage sets for ion-shuttling operations with a constant secular frequency under the restrictions of DAC output ranges. Our experimental results demonstrate that the DAC system can generate potentials with a secular frequency of $2\pi \times 500$ kHz, which is twice of that achievable when the output range is restricted to ± 10 V, a typical limitation of conventional DACs. During the shuttling operation, the desired potential at each transport step was validated by measuring the secular frequency of the trapped ions.

ACKNOWLEDGMENTS

This work was supported by JST Moonshot R & D (Grant Number JPMJMS2063), JST COINEXT (Grant Number JPMJPF2014), JST Moonshot R & D (Grant Number JPMJMS226A), and MEXT Q-LEAP (Grant Number JP-MXS0120319794).

DATA AVAILABILITY STATEMENT

The data that support the findings of this study are available from the corresponding author upon reasonable request.

REFERENCES

- ¹C. D. Bruzewicz, J. Chiaverini, R. McConnell, and J. M. Sage, “Trapped-ion quantum computing: Progress and challenges,” *Applied Physics Reviews* **6**, 021314 (2019).
- ²P. Wang, C.-Y. Luan, M. Qiao, M. Um, J. Zhang, Y. Wang, X. Yuan, M. Gu, J. Zhang, and K. Kim, “Single ion qubit with estimated coherence time exceeding one hour,” *Nature communications* **12**, 233 (2021).
- ³C. J. Ballance, T. P. Harty, N. M. Linke, M. A. Sepiol, and D. M. Lucas, “High-fidelity quantum logic gates using trapped-ion hyperfine qubits,” *Phys. Rev. Lett.* **117**, 060504 (2016).
- ⁴J. P. Gaebler, T. R. Tan, Y. Lin, Y. Wan, R. Bowler, A. C. Keith, S. Glancy, K. Coakley, E. Knill, D. Leibfried, and D. J. Wineland, “High-fidelity universal gate set for $^9\text{Be}^+$ ion qubits,” *Phys. Rev. Lett.* **117**, 060505 (2016).
- ⁵C. M. Löschnauer, J. M. Toba, A. C. Hughes, S. A. King, M. A. Weber, R. Srinivas, R. Matt, R. Nourshargh, D. T. C. Allcock, C. J. Ballance, C. Matthiesen, M. Malinowski, and T. P. Harty, “Scalable, high-fidelity all-electronic control of trapped-ion qubits,” (2024), arXiv:2407.07694 [quant-ph].
- ⁶J.-S. Chen, E. Nielsen, M. Ebert, V. Inlek, K. Wright, V. Chaplin, A. Maksymov, E. Páez, A. Poudel, P. Maunz, and J. Gamble, “Benchmarking a trapped-ion quantum computer with 30 qubits,” *Quantum* **8**, 1516 (2024).
- ⁷I. Pogorelov, T. Feldker, C. D. Marciniak, L. Postler, G. Jacob, O. Krieglsteiner, V. Podlesnic, M. Meth, V. Negnevitsky, M. Stadler, B. Höfer, C. Wächter, K. Lakhmanskiy, R. Blatt, P. Schindler, and T. Monz, “Compact ion-trap quantum computing demonstrator,” *PRX Quantum* **2**, 020343 (2021).
- ⁸D. Keilpinski, C. Monroe, and D. J. Wineland, “Architecture for a large-scale ion trap quantum computer,” *Nature* **417**, 709–711 (2002).
- ⁹V. Kaushal, B. Lekitsch, A. Stahl, J. Hilder, D. Pijn, C. Schmiegelow, A. Bermudez, M. Müller, F. Schmidt-Kaler, and U. Poschinger, “Shuttling-based trapped-ion quantum information processing,” *AVS Quantum Science* **2**, 014101 (2020).
- ¹⁰J. M. Pino, J. M. Dreiling, C. Figgatt, J. P. Gaebler, S. A. Moses, M. S. Allman, C. H. Baldwin, M. Foss-Feig, D. Hayes, K. Mayer, C. Ryan-Anderson, and B. Neyenhuis, “Demonstration of the trapped-ion quantum CCD computer architecture,” *Nature* **592**, 209–213 (2021).
- ¹¹S. A. Moses *et al.*, “A race-track trapped-ion quantum processor,” *Phys. Rev. X* **13**, 041052 (2023).
- ¹²M. Malinowski, D. T. C. Allcock, and C. J. Ballance, “How to wire a 1000-qubit trapped-ion quantum computer,” *PRX Quantum* **4**, 040313 (2023).
- ¹³R. Reichle, D. Leibfried, R. Blakestad, J. Britton, J. Jost, E. Knill, C. Langer, R. Ozeri, S. Seidelin, and D. Wineland, “Transport dynamics of single ions in segmented microstructured paul trap arrays,” *Fortschritte der Physik* **54**, 666–685 (2006).
- ¹⁴A. H. Nizamani and W. K. Hensinger, “Optimum electrode configurations for fast ion separation in microfabricated surface ion traps,” *Applied Physics B* **106**, 327–338 (2012).
- ¹⁵G. Huber, T. Deuschle, W. Schnitzler, R. Reichle, K. Singer, and F. Schmidt-Kaler, “Transport of ions in a segmented linear paul trap in printed-circuit-board technology,” *New Journal of Physics* **10**, 013004 (2008).
- ¹⁶R. Bowler, J. Gaebler, Y. Lin, T. R. Tan, D. Hanneke, J. D. Jost, J. P. Home, D. Leibfried, and D. J. Wineland, “Coherent diabatic ion transport and separation in a multizone trap array,” *Phys. Rev. Lett.* **109**, 080502 (2012).
- ¹⁷A. Walther, F. Ziesel, T. Ruster, S. T. Dawkins, K. Ott, M. Hettrich, K. Singer, F. Schmidt-Kaler, and U. Poschinger, “Controlling fast transport of cold trapped ions,” *Phys. Rev. Lett.* **109**, 080501 (2012).
- ¹⁸H. A. Fürst, M. H. Goerz, U. G. Poschinger, M. Murphy, S. Montangero, T. Calarco, F. Schmidt-Kaler, K. Singer, and C. P. Koch, “Controlling the transport of an ion: classical and quantum mechanical solutions,” *New Journal of Physics* **16**, 075007 (2014).
- ¹⁹M. G. House, “Analytic model for electrostatic fields in surface-electrode ion traps,” *Phys. Rev. A* **78**, 033402 (2008).
- ²⁰S. Gulde, D. Rotter, P. Barton, F. Schmidt-Kaler, R. Blatt, and W. Hoger-vorst, “Simple and efficient photo-ionization loading of ions for precision ion-trapping experiments,” *Applied Physics B* **73**, 861–863 (2001).
- ²¹D. M. Lucas, A. Ramos, J. P. Home, M. J. McDonnell, S. Nakayama, J.-P. Stacey, S. C. Webster, D. N. Stacey, and A. M. Steane, “Isotope-selective photoionization for calcium ion trapping,” *Phys. Rev. A* **69**, 012711 (2004).
- ²²M. Frank and P. Wolfe, “An algorithm for quadratic programming,” *Naval Research Logistics Quarterly* **3**, 95–110 (1956).
- ²³H. Nägerl, D. Leibfried, F. Schmidt-Kaler, J. Eschner, and R. Blatt, “Coherent excitation of normal modes in a string of Ca^+ ions,” *Opt. Express* **3**, 89–96 (1998).